AAPS PharmSciTech, Vol. 12, No. 4, December 2011 (© 2011)
DOI: 10.1208/s12249-011-9704-0

Research Article

Theme: Advances in Pharmaceutical Excipients Research and Use: Novel Materials, Functionalities and Testing
Guest Editors: Otilia Koo, Thomas Farrell, Allison Radwick, and Sameer Late

Physicochemical Characterization and Water Vapor Sorption of Organic Solution Advanced Spray-Dried Inhalable Trehalose Microparticles and Nanoparticles for Targeted Dry Powder Pulmonary Inhalation Delivery

Xiaojian Li[1] and Heidi M. Mansour[1,2]

Received 1 June 2011; accepted 29 September 2011; published online 25 October 2011

Abstract. Novel advanced spray-dried inhalable trehalose microparticulate/nanoparticulate powders with low water content were successfully produced by organic solution advanced spray drying from dilute solution under various spray-drying conditions. Laser diffraction was used to determine the volumetric particle size and size distribution. Particle morphology and surface morphology was imaged and examined by scanning electron microscopy. Hot-stage microscopy was used to visualize the presence/absence of birefringency before and following particle engineering design pharmaceutical processing, as well as phase transition behavior upon heating. Water content in the solid state was quantified by Karl Fisher (KF) coulometric titration. Solid-state phase transitions and degree of molecular order were examined by differential scanning calorimetry (DSC) and powder X-ray diffraction, respectively. Scanning electron microscopy showed a correlation between particle morphology, surface morphology, and spray drying pump rate. All advanced spray-dried microparticulate/nanoparticulate trehalose powders were in the respirable size range and exhibited a unimodal distribution. All spray-dried powders had very low water content, as quantified by KF. The absence of crystallinity in spray-dried particles was reflected in the powder X-ray diffractograms and confirmed by thermal analysis. DSC thermal analysis indicated that the novel advanced spray-dried inhalable trehalose microparticles and nanoparticles exhibited a clear glass transition (T_g). This is consistent with the formation of the amorphous glassy state. Spray-dried amorphous glassy trehalose inhalable microparticles and nanoparticles exhibited vapor-induced (lyotropic) phase transitions with varying levels of relative humidity as measured by gravimetric vapor sorption at 25°C and 37°C.

KEY WORDS: microparticulate/nanoparticulate inhalable powders; non-reducing sugar excipient; organic solution advanced spray drying; respiratory delivery; trehalose.

INTRODUCTION

Pulmonary inhalation drug delivery offers attractive advantages in delivering high concentrations of drug directly to the disease site in the lungs while minimizing systemic bioavailability (1). Many mortal lung infections such as those in cystic fibrosis reside in both the mid and and low airway regions (2–5). Therefore, local drug delivery for treatment can be enhanced through the use of microparticles and nanoparticles (6,7) in pulmonary delivery (8). These particles can efficiently deposit in the lungs by physical sedimentation and diffusion particle deposition mechanisms, respectively (9). Three main delivery systems have been utilized for the inhalation of aerosolized drugs, namely, nebulizers, pressurized metered-dose inhalers (pMDIs) and dry powder inhalers (DPIs) (1,10). Various interparticulate interactions (11) influence DPI dispersion performance and include van der Waals, capillary, and electrostatic forces (12–14).

Freeze drying and spray drying are the two most common processes which allow the conversion of the formulation from the liquid state to the solid state particularly for dry powder inhalation formulation design and development (10). Nevertheless, freezing and thermal stresses associated with both processes are often observed. Therefore, cryoprotectants (15) and thermoprotectants (16) are frequently incorporated in the formulation for the purpose of protection of drug stability. Carbohydrates (17,18) are commonly used as cryoprotectants and thermoprotectants. Trehalose can be successfully included in inhalation formulations that contain biotherapeutic drugs (biologics) (19), including aqueous solution spray-freeze-dried formulations to produce large trehalose particles for nasal vaccination delivery (20). It has many advantages over other sugars, such as less hygroscopicity, an absence of internal hydrogen bonds

[1] Department of Pharmaceutical Sciences—Drug Development Division, University of Kentucky College of Pharmacy, 789 S. Limestone Street, Lexington, Kentucky 40536-0596, USA.
[2] To whom correspondence should be addressed. (e-mail: heidi.mansour@uky.edu)

that allows more flexible formation of hydrogen bonds with drugs, low chemical reactivity, and high glass transition temperature (21). Moreover, trehalose dihydrate has notable similarities to the pulmonary sugar carrier, lactose monohydrate, as both are crystalline disaccharides and both are hydrates. Notable differences with lactose monohydrate are that trehalose dihydrate is a non-reducing sugar, and hence, it is not susceptible to the solid-state chemical degradation Maillard reaction. Additionally, it is not metabolized by bacteria due to its non-reducing property. Freeze-dried trehalose (22–24) and aqueous solution spray-dried trehalose (24–26) have been reported for non-inhalation dry powder dosage forms.

Exploring alternative sugar carriers for pulmonary inhalation formulation is of considerable interest (27). It has been demonstrated that trehalose can effectively improve dry powder aerosolization by increasing the fine particle fraction (28). Recently, trehalose dihydrate as an aerosol drug carrier for dry powder inhalation delivery has been systematically studied and was found to be an effective alternative to lactose monohydrate carrier (29). Additionally, trehalose has been used a lyoprotectant stabilizing excipient in dry powder inhalation aerosol formulations (30).

The unique features of spray drying involve the ability of particle design, formation, and drying in a continuous single-step that starts with a liquid and ends with the powder formulation. It provides the theoretical framework for a rational design of structured aerosol particles (8,10,31). Typically, the spray-drying process consists of atomization of feed into a spray, spray–air contact, solvent evaporation of the spray, and separation of the dried particles from the drying air (32). However, particle engineering requires a deeper understanding of particle formation processes since many process and formulation variables need to be tuned correctly to achieve the desired structured particles for inhalation.

By using organic solvent in feedstock with no water present, much lower moisture content and significantly smaller particle size can be achieved down to ~400 nm. The non-aqueous nature and inherently lower surface tension of an organic solvent combined with a low (dilute) solute concentration enables particle production in the solid state down to the inhalable nanometer size range while maintaining a unimodal and narrow particle size distribution in the solid state. To the authors' knowledge, this study is the first to use and report this novel approach to rationally design and produce inhalable dry powder microparticles/nanoparticles for pulmonary delivery. These novel particles are produced by organic solution advanced spray drying from dilute solution under rationally chosen spray drying conditions. The goal of this study was to produce and optimize low water content trehalose microparticles and nanoparticles to be suitable for pulmonary delivery as dry powder inhalers (DPIs) and to comprehensively and systematically investigate the physicochemical and particle properties of spray-dried and raw trehalose particles.

MATERIALS AND METHODS

Materials

The chemical structure of D-(+)-trehalose dihydrate ($C_{12}H_{26}O_{13}$; molecular weight, 378.33 g/mol; ≥98.5% purity, Sigma-Aldrich Inc., St. Louis, MO) is shown in Fig. 1

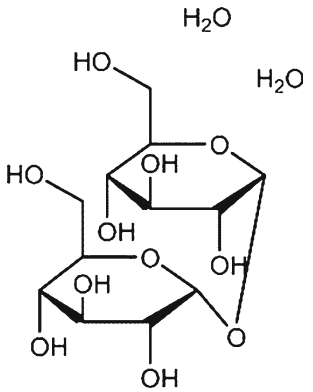

Fig. 1. The chemical structure of D-(+)-trehalose dihydrate

(ChemDraw Ultra 10.0, ChemOffice, Cambridge, MA) and its molecular model has been previously reported by Mansour and Hickey (30). Methanol (HPLC grade) and chloroform were obtained from Fisher Scientific (Fair Lawn, New Jersey). HYDRANAL®-Coulomat AD was from Sigma-Aldrich (St. Louis, Missouri). AQUA STAR methanol was from EMD chemical Inc. (Gibbstown, New Jersey).

Methods

Organic Solution Advanced Spray Drying from Dilute Solution

The advanced spray-drying process was performed using the Büchi Mini Spray Dryer B-290 (Büchi, Switzerland) coupled with the Inert Loop B-295 (Büchi, Switzerland) and the high-performance (HP) cyclone (Büchi, Switzerland). The spray-drying process was in closed mode. The feeding solution was prepared by dissolving D-(+)-trehalose dihydrate in methanol to form a dilute solution with a concentration of 0.3% *w/v*. The following spray-drying conditions were rationally chosen and used: atomization gas flow rate was 600 L/h; aspiration rate was 35 m^3/h; three different pump rates were rationally chosen to represent the "high", "medium", and "low" pump rates which were 100% (30 mL/min), 50% (15 mL/min), and 10% (3 mL/min), respectively. The inlet temperature was set at 150°C and this represents the temperature maintained the first drying process. The corresponding outlet temperature for the secondary drying process at the three different pump rates were 39°C (high pump rate), 45°C (medium pump rate), and 53°C (low pump rate). The nozzle diameter of the stainless steel nozzle was 0.7 mm. The spray-dried (SD) particles were separated from the ultra-high-purity (UHP) nitrogen drying gas in a high-performance cyclone and collected in a sample collector. UHP grade compressed nitrogen gas from Scott-Gross (Lexington, Kentucky) was used as the spray-drying gas during closed mode spray drying.

All spray-dried powders were carefully stored in sealed glass vials that were stored in sealed glass desiccators over Indicating Drierite/Drierite™ desiccant at 25°C under ambient pressure.

Laser Light Diffraction Particle Sizing and Size Distribution

The mean size and size distribution of the particles in chloroform suspension were determined by ultraviolet laser

diffraction of nanoparticle size analyzer SALD-7101 (Shimadzu, Japan). Using the method previously reported by Mansour *et al.* (29), powders were dispersed in chloroform and ultrasonicated for 10 s (Branson 5210 Ultrasonicator Bath, Danbury, Connecticut) to break up the agglomerates without reducing the primary particle size before particle size measurements were carried out. Sample particle dispersion was immediately transferred to the particle size measuring quartz glass cell under stirred conditions. The low refractive index 1.60–0.10 was used. Number-based dimension of particle amount distribution was obtained for samples. In addition to acquiring the particle size distributions, the D_{v10}, D_{v50}, and D_{v90} parameters were measured. The span value was calculated using the equation defined as $[(D_{v90}-D_{v10})/D_{v50}]$.

Scanning Electron Microscopy

The shape and surface morphology of particles was evaluated by scanning electron microscopy (SEM), using a Hitachi S-800 microscope (Tokyo, Japan). Samples were placed on double-sided adhesive carbon tabs (TedPella, Inc.) which were adhered to aluminum stubs (TedPella, inc.) and were coated with gold/palladium alloy thin film using a Hummer VI sputtering system from Technics. The coating process was operated at 10 AC mA for 3 min. The electron beam with an accelerating voltage of 20 kV was used at a working distance of 30 mm. SEM images were captured using Evex NanoAnalysis software. Several magnification levels were used.

Powder X-ray Diffraction

Powder X-ray diffraction patterns of powder samples were measured by a Rigaku Multiflex X-ray diffractometer (Japan) with a slit-detector Cu Kα radiation (40 kV, 44 mA, and λ=1.5406 Å) source. Scan range was 5.0–50.0 $(2\theta)^{o}$ with a scan rate of 2.00°/min at ambient temperature. The sample was placed on a horizontal quartz glass sample holder plate.

Differential Scanning Calorimetry

Thermal analysis and phase transition measurements were carried out using a TA Q200 differential scanning calorimetry (DSC) system (TA Instruments, New Castle, Delaware) equipped with T-Zero® technology and an automated computer-controlled RSC-90 cooling accessory (TA Instruments, New Castle, Delaware). Approximately 3 mg of powder was carefully weighed into hermetic anodized aluminum T-Zero® DSC pans (TA Instruments T-Zero®, New Castle, Delaware) and were sealed with the T-Zero® hermetic sealer (TA Instruments New Castle, Delaware). UHP nitrogen gas (Scotts Gross, Lexington, KY) was used as the purging gas at a purge rate of 50 mL/min. The heating range was 10–250°C at a heating scan rate of 5.00°C/min.

Karl Fisher Coulometric Titration

The water content of all powders was chemically quantified by Karl Fisher (KF) coulometric titration. The measurements were performed with a 737 KF Coulometer coupled with 703 Ti Stand (Metrohm Ltd., Antwerp, Belgium). Approximately 10 mg of powder was dissolved in AQUASTAR® anhydrous methanol in a 5-mL volumetric flask. The sample solution was injected into the reaction cell that contained HYDRANAL® KF reagent. The water content was then calculated.

Gravimetric Vapor Sorption

Water vapor absorption isotherms were measured gravimetrically using an automated ultra-high-sensitivity Cahn microelectronic balance (Thermoscientific Instruments) coupled to a computerized VTI SGA-CX symmetric vapor sorption analyzer (VTI Corporation, Hialeah, Florida). All measurements were taken at 25°C and 37°C (i.e., biological temperature) at using a sample size of 1.0–1.5 mg. Samples were subjected to drying treatment at 25°C (for absorption at 25°C) and at 37°C (for absorption at 37°C) under UHP nitrogen gas (Scotts Gross, Lexington, KY) for 7 h. At the end of the drying cycle, the samples were exposed to an automated computerized sequence of increasing relative humidity (RH) in steps of 5% RH. The RH range was from 0% RH to 95% RH. Sample data acquisition was collected in 2-min intervals. The equilibrium criterion was a weight change of ≤0.03% (*w*/*w*) in a 10-min interval, per manufacturer recommendations and as reported previously by Mansour and Zografi (33).

Hot-Stage Microscopy Under Cross-Polarizers

Hot-stage microscopy (HSM) studies were performed under OLYMPUS BX51 polarized microscope (Olympus, Japan) equipped with an INSTEC STC200 heating unit and an INSTEC HCS302 hot stage (Boulder, Colorado). The polarized light was filtered by a γ 530 nm U-TP530 (Olympus, Japan) filter lens. Powder samples were mounted on a cover glass and heated from 25°C to 250°C at a heating rate of 5°C/min. The heating program was controlled by WinTemp software. Images were digitally captured by a SPOT Insight digital camera (Diagnostic Instruments, Inc.).

RESULTS

Laser Light Diffraction Particle Sizing and Size Distribution

The particle sizing data and calculated span values are tabulated in Table I. The particle size distributions for all spray-dried powders were unimodal with narrow particle distribution, as reflected in the span values. The raw trehalose dihydrate had a large volume-median particle size of ~60 μm as tabulated in Table I. Great reduction of particle size was achieved by organic solution advanced spray drying from dilute solution to create microparticulate/nanoparticulate powders that are in the respirable size range.

Scanning Electron Microscopy

The particle morphology and surface morphology (i.e., surface roughness) of the samples were visualized and analyzed using SEM. As shown in Fig. 2, smooth and

Table I. Particle size parameters of SD trehalose and raw trehalose dihydrate particles (mean ± SD, n=3)

	Samples	D_{v10} (μm)	D_{v50} (μm)	D_{v90} (μm)	Span value
SD	10% feeding rate	0.549±0.003	0.752±0.008	1.177±0.012	0.836±0.010
	50% feeding rate	0.710±0.006	0.993±0.013	1.544±0.019	0.840±0.030
	100% feeding rate	0.646±0.109	0.947±0.071	1.648±0.228	1.080±0.455
	Raw	35.139±2.602	59.854±3.296	110.460±1.568	1.263±0.122

spherical particles were produced by 10% SD pump feeding rate. However, as the pump % feeding rate approached 100% (high), the surface roughness increased and the proportion of irregular particles also increased. Interestingly, raisin-like dimpled particles were produced at the high pump % feeding rate of 100%. SEM analysis of the particle size agreed with the laser sizing data in that all spray-dried powders were in the suitable size range for inhalation delivery, in addition to having suitable particle morphology. Contrastingly, the raw trehalose dihydrate particles were much larger (too large for pulmonary inhalation delivery) and non-spherical with a smooth but rectangular shape which are not suitable for inhalation delivery.

Powder X-ray Diffraction

Powder X-ray diffraction patterns (Fig. 3) indicated that the organic solution spray-drying process produced amorphous phase trehalose particles, as exemplified by the absence of sharp peaks and the presence of the characteristic non-crystalline "halo" which can be attributed to the loss of crystal character following the loss of the two bound water molecules (i.e., tightly bound to the crystal lattice by thermodynamically favorable H-bonding) during the organic solution advanced spray-drying process from dilute solution. In contrast, the raw trehalose dihydrate had many intense peaks indicative of the presence of long-range molecular

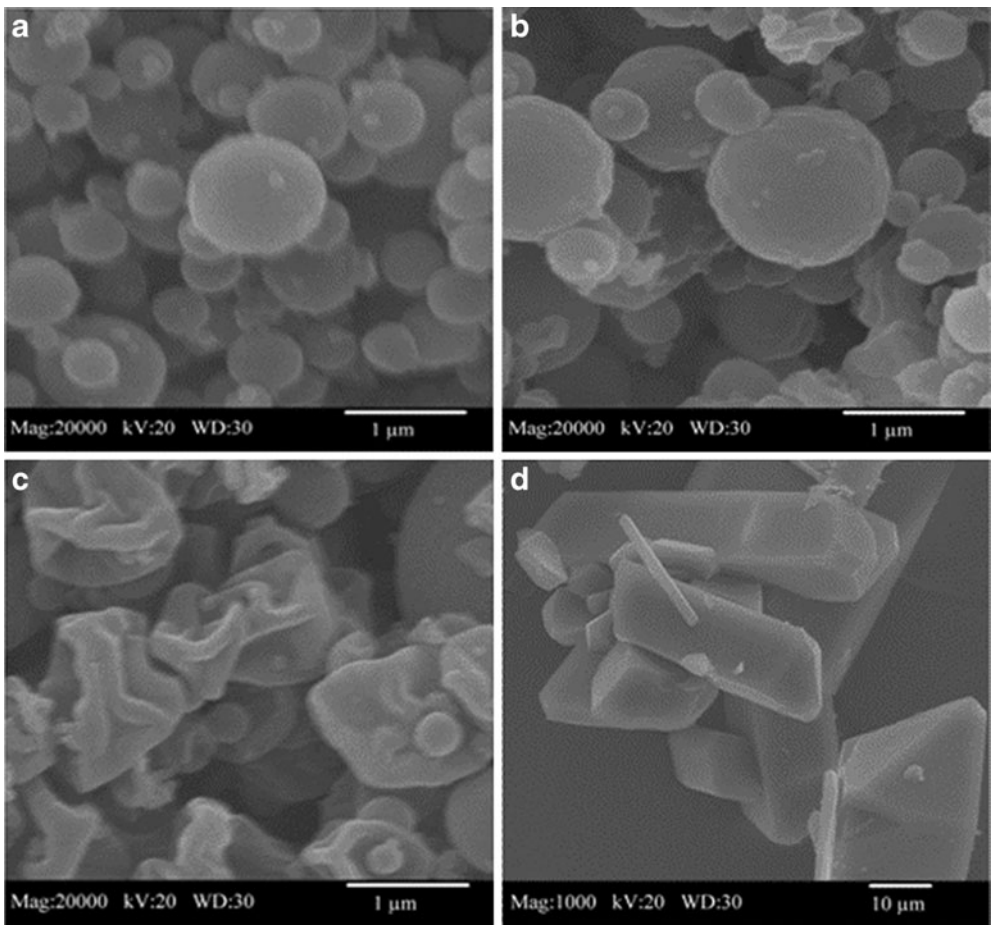

Fig. 2. SEM micrographs of spray-dried trehalose and raw trehalose dihydrate particles. **a** SD trehalose from 10% feeding rate, magnification ×20,000; **b** SD trehalose from 50% feeding rate, magnification ×20,000; **c** SD trehalose from 100% feeding rate, magnification ×20,000; **d** D-(+)-trehalose dihydrate, magnification ×1,000

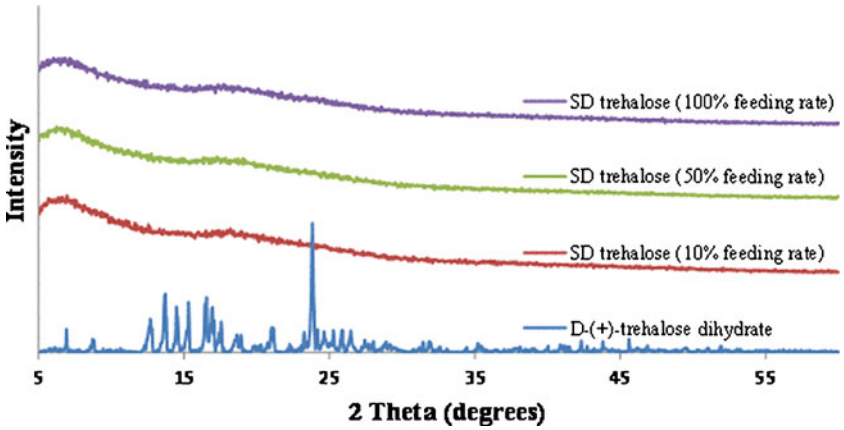

Fig. 3. Powder X-ray diffractograms of SD trehalose and raw trehalose dihydrate particles

order due to crystallinity. The peaks represented that the raw trehalose dihydrate was highly crystalline which is in a good agreement with the University of Cambridge database and by results reported by Mansour *et al.* (29). The loss of characteristic crystalline peaks ("halo") is in good agreement with previous reports on aqueous solution spray-dried trehalose under different conditions (34).

Differential Scanning Calorimetry

The thermograms obtained from raw trehalose dihydrate and SD trehalose are shown in Fig. 4. There were three endothermic peaks observed for raw trehalose dihydrate which are characteristic for order-to-disorder thermotropic phase transitions. Similar DSC thermograms were obtained for single crystals of trehalose dihydrate (35) and for raw trehalose dihydrate powder (20). The two endothermic order-to-disorder peaks at ~100°C and 140°C correspond to two dehydration processes due to the loss of unbound water at ~100°C (i.e., vaporization of unbound water) and vaporization of the bound water molecules at 140°C which vaporize at a temperature significantly greater than 100°C due to thermodynamically favorable H-bonding of the water molecules within the trehalose dihydrate crystal lattice. The third endothermic order-to-disorder peak at 210°C represented the fusion of anhydrous β form of trehalose (36). All SD trehalose samples showed an amorphous glassy-to-rubbery phase transition, T_g, (i.e., characteristic baseline shift) at ~50°C, followed by an exothermic disorder-to-order phase transition near 95°C which suggests crystallization at T_c from the amorphous rubbery state. A small endothermic order-to-disorder peak was observed in the temperature range of 140–150°C for the SD trehalose samples. To the authors' knowledge, this peak has not been reported previously in the literature. The fusion of the β form of trehalose was observed in this same temperature range as the raw trehalose dihydrate.

Karl Fisher Coulometric Titration

The water content data are plotted in Fig. 5. The mean total water content of raw trehalose dihydrate was 9.62% (*w*/*w*) with a standard deviation (SD) value of ±0.08% (*w*/*w*). This data is in excellent agreement with the literature (35). By comparing the theoretical minimum water content of raw trehalose dihydrate (9.52% (*w*/*w*)), it suggested that there was a trace amount of water (0.1% (*w*/*w*)) adsorbed to its surface, as the sample was stored under ambient conditions (approximately 55% RH and 25°C). As stated in the Methods section, all spray-dried trehalose powders were stored in a sealed glass desiccator containing Drierite®/Indicating Drierite® desiccant under room temperature of 25°C. The water content values were 0.73% (*w*/*w*) (SD=±0.25% (*w*/*w*)), 0.86% (*w*/*w*) (SD=±0.09% (*w*/*w*)), and 1.51% (*w*/*w*) (SD=±0.01% (*w*/*w*)) for samples produced by 10% (low), 50% (medium), and 100% (high) pump feeding rates, respectively.

Gravimetric Vapor Sorption

The gravimetric vapor sorption isotherms of the three spray-dried trehalose and raw trehalose dihydrate samples are plotted in Fig. 6a. From 0% to 55% of RH, all three SD samples underwent a rising curve with respect to their mass changes, reflecting an increasing capability of water vapor uptake. Interestingly, a transition point of water vapor sorption took place at 30% RH. This may be due to the SD trehalose samples passing through the lyotropic vapor-induced glass transition, from lower molecular mobility of the glassy state to higher molecular mobility of the rubbery state. The uptake of water vapor of the sample continued to increase after the lyotropic vapor-induced glass transition. The amorphous trehalose relaxed to its more stable crystalline state through crystallization at 55–60% RH and the water vapor sorption capacity decreased sharply over a very narrow RH range followed by a plateau in vapor absorption. A slight desorption of water was observed for SD trehalose samples after 60% RH followed by the plateau region suggestive of the recystallization process from the amorphous state to the crystalline state. It also suggests the transition from unbound water to bound water, as occurs during the process of crystallization.

The water vapor sorption isotherms of SD trehalose particles (50% pump feeding rate) at 25°C and 37°C were measured as shown in Fig. 6b. The water vapor absorption isotherm at 37°C appeared to reach the equilibrium faster than at 25°C in terms of RH%. For example, the SD amorphous trehalose reached its highest weight change percentage at 50% RH at 37°C *vs.* 55%

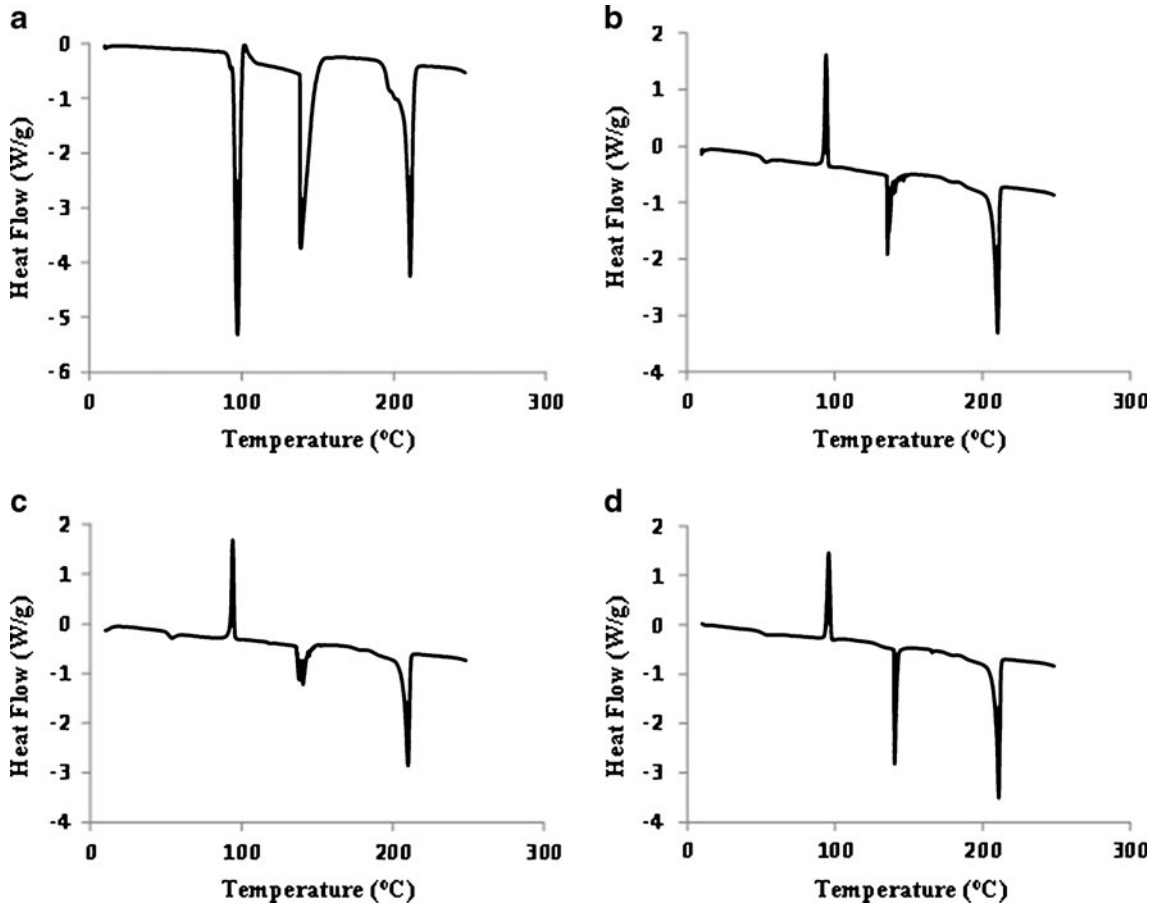

Fig. 4. DSC thermograms of SD trehalose and raw trehalose dihydrate particles. **a** D-(+)-trehalose dihydrate; **b** SD trehalose (10% feeding rate); **c** SD trehalose (50% feeding rate); **d** SD trehalose (100% feeding rate)

RH at 25°C. In addition, the SD amorphous trehalose exhibited more water vapor uptake at 37°C than at 25°C across the whole RH% range studied while retaining the similar isothermal profile trend.

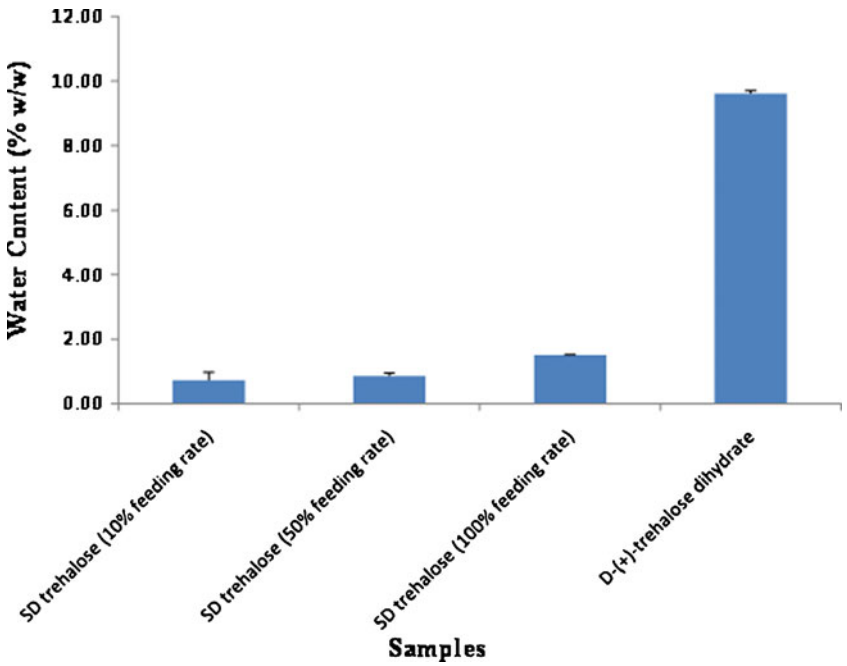

Fig. 5. Water content of SD trehalose and raw trehalose dihydrate particles

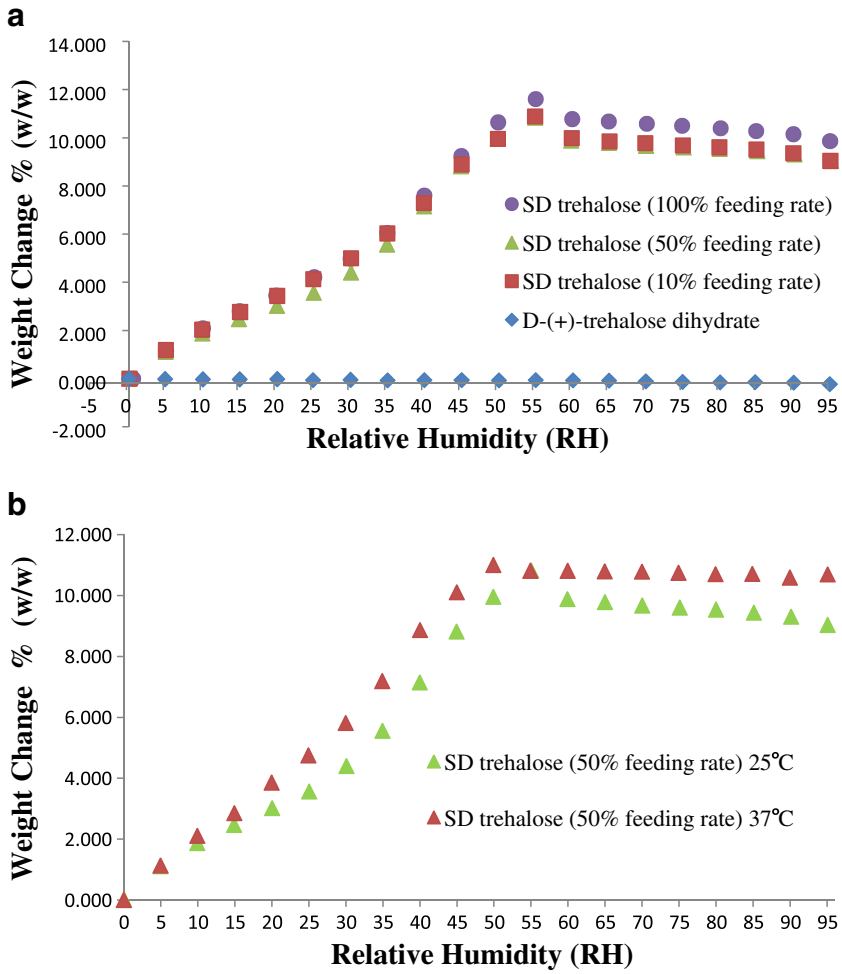

Fig. 6. Water vapor absorption isotherms of SD trehalose and raw trehalose dihydrate particles (weight (%) *vs* relative humidity (*RH*)): **a** comparison of water vapor absorption between SD trehalose and raw trehalose dihydrate particles at 25°C; **b** comparison of water vapor absorption of SD trehalose particles (50% feeding rate) at 25°C and 37°C

Hot-Stage Microscopy Under Cross-Polarizers

The HSM images of raw trehalose dihydrate upon heating are shown in Fig. 7. Under cross-polarized light, the birefrigency of raw trehalose dihydrate were observed at 25°C and 37°C. The birefrigency of raw trehalose dihydrate started to diminish at 108°C and disappeared finished at 116°C. This phase transition may correspond to its first endothermic order-to-disorder phase transition, as seen in Fig. 4 for raw trehalose dihydrate. This may be due to the first dehydration process, i.e., loss of unbound water. As seen in Fig. 7, the crystal shape was retained during this transition. However, during the second endothermic order-to-disorder phase transition, the crystal shape disappeared in the temperature range 146–160°C. Subtle birefringency reemerged in the temperature range of 200–227°C which may suggest a subtle recrystallization event which was not observed in the DSC thermogram. Melting was visualized in the temperature range of 231–234°C as evident by liquid droplet formation.

SD trehalose from 50% feeding rate (Fig. 8) showed dark agglomerates lacking birefringency at 25°C and 37°C, as would be expected for non-crystalline amorphous materials. The recrystallization of SD trehalose with increasing temperature was not visually evident due to the small particle size of SD trehalose (Table I). The first phase transition visualized by HSM appears to correlate with the small order-to-disorder endotherm (perhaps due to a metastable phase transition or a pretransition), as observed in the DSC thermogram at 140–150°C in Fig. 4c. The melting process occurred at higher temperatures as evident by liquid droplet formation seen in the micrographs.

DISCUSSION

The present work demonstrates that low water content trehalose microparticles and nanoparticles with particle properties necessary for inhalation dry powder delivery can be successfully produced by organic solution advanced spray drying from dilute solution using rationally selected spray-drying conditions. By using low concentration of organic solvent solution, the unimodal narrow particle size distribution of SD trehalose microparticulate/nanoparticulate powders was achieved. The unimodal narrow particle size distribution is critical for pulmonary dry powder inhalation, as it enables the particles to target a specific lung region

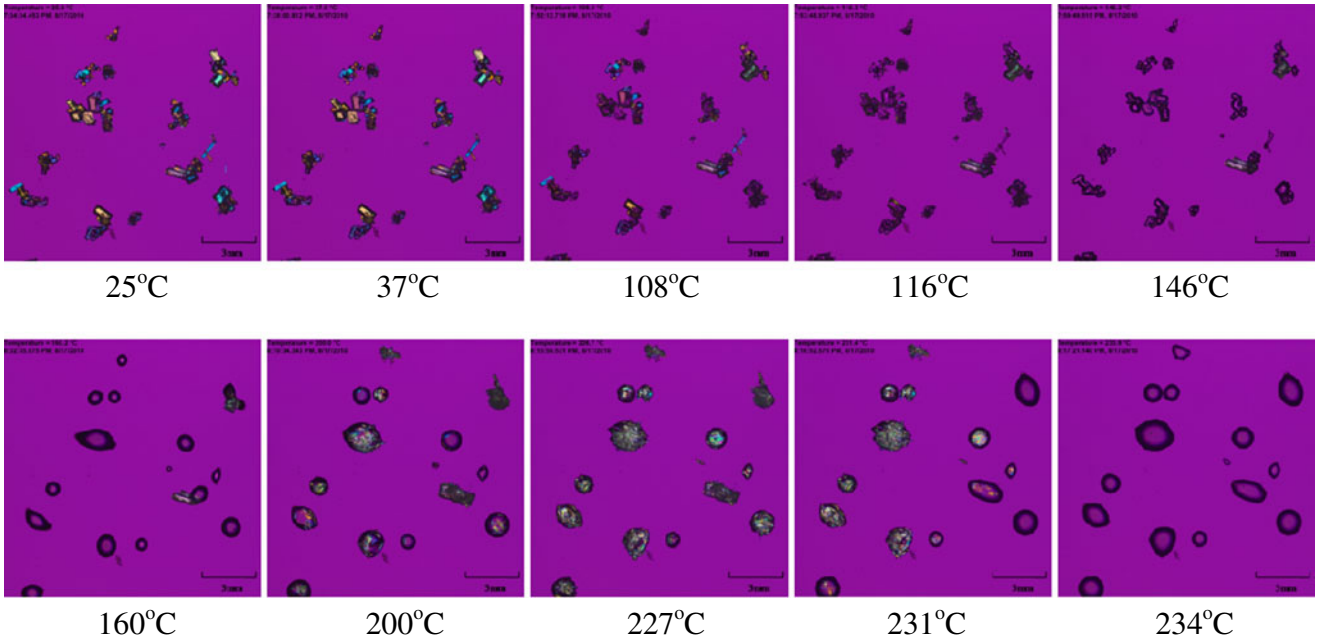

Fig. 7. HSM of raw trehalose dihydrate particles

which consequently can lower the therapeutic dose. In addition, the water content of final product can be reduced via spray drying the organic solution of trehalose instead of water solution. Since the size of inhalable particles is small, residual water can have a significant influence on the dispersion of dry powder during aerosolization through capillary force (12). However, the water content of SD trehalose increased a bit as the pump rate increased but was still at the level that is considered to be low.

The surface morphology, as visualized by SEM, changed with increasing pump feeding rates. Specifically, smooth particles and corrugated particles were produced by low feeding rate and high feeding rate, respectively. Research studies (37,38) have demonstrated that the particle morphology of dry powder can impact the aerosol performance.

From the PXRD and DSC data, they showed that the organic solution advanced spray-drying process from dilute solution changed raw crystalline trehalose dihydrate into SD amorphous glassy trehalose. The change of pump rate did not significantly affect the PXRD and DSC data for SD trehalose particles. However, DSC thermal analysis for SD trehalose appears to suggest that amorphous rubbery trehalose crystallizes to a relatively more ordered phase at a T_c ~95°C, as seen by the distinct disorder-to-order exothermic phase transition present in the thermograms.

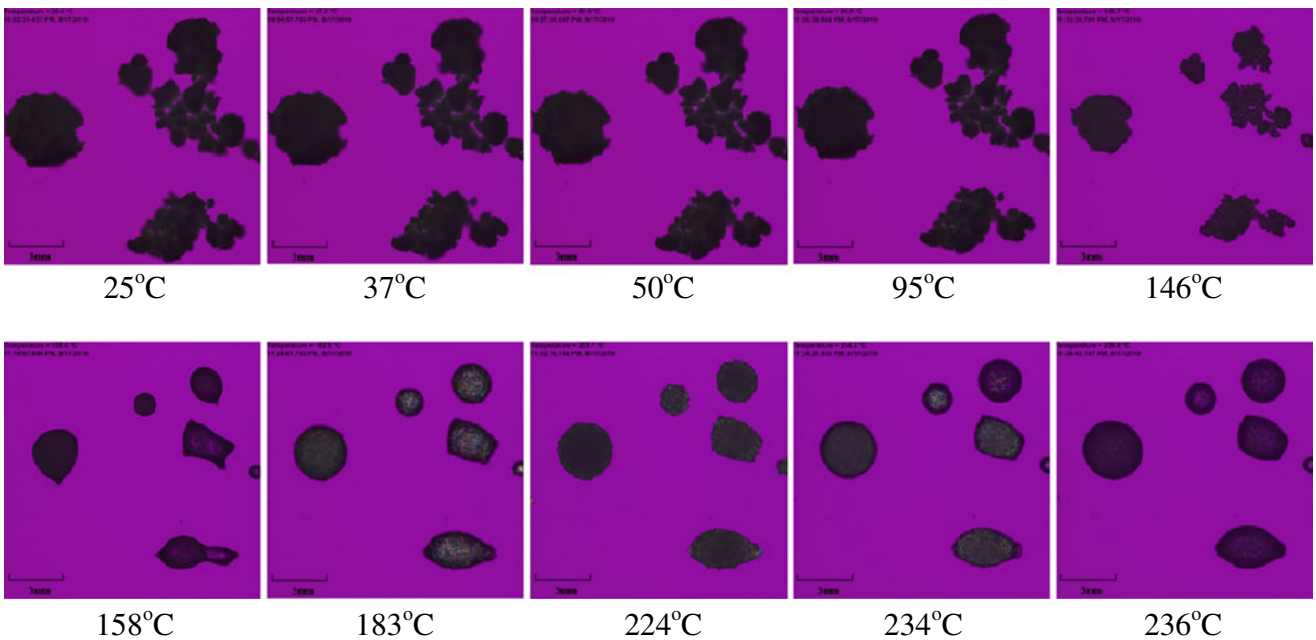

Fig. 8. HSM of SD trehalose particles (50% feeding rate)

Gravimetric vapor sorption study illustrated water vapor lyotropic effect on SD trehalose particles microparticulate/nanoparticulate powders. A vapor-induced phase transition suggestive of a glass transition occurred at 30% RH, after which point water vapor uptake continued to increase up to ~55% RH. The crystallization process appeared to occur during vapor absorption in the RH range of 55–60% RH, as evident by the sharp decrease in water vapor uptake over a narrow RH range followed by the plateau in vapor uptake. It is generally recognized that temperature and RH are two important factors on the phase transition behavior and stability on amorphous phases (39,40). As expected for crystalline hydrate powders, raw trehalose dihydrate did not absorb any significant amounts of water vapor over the entire range of RH, as it is in its thermodynamically stable state.

Figure 9 shows water vapor uptake lyotropic phase behavior at 25°C (ambient temperature) and 37°C (biological temperature) on a molar basis for stoichiometric water content analysis and insight. Figure 9a shows that the raw trehalose dihydrate did not exhibit any significant water vapor uptake on a molar basis. This is expected for crystalline materials especially for crystalline hydrate powders, as crystalline materials are in a relatively lower thermodynamic energy state.

All spray-dried trehalose amorphous glassy particles, produced using three different pump feeding rates, had similar water vapor sorption profiles but were significantly greater than raw crystalline trehalose dihydrate, as shown in Fig. 9a. The stoichiometric molar ratio reached to 2.1 (i.e., dihydrate) at 55% RH and remained at this level in the plateau region which suggests a lyotropic phase transition from the amorphous rubbery state (i.e., higher energy state) to the thermodynamically stable dihydrate crystal (lower energy state). It decreased slightly followed by a plateau region. There appears to be a slight ratio decrease for SD trehalose at 25°C starting from the crystallization point, reaching to 1.8 moles (i.e., dihydrate) in the plateau region. Figure 9b shows that the SD trehalose particles had a lesser decrease in the stoichiometric molar ratio at 37°C (biological temperature) at the recrystallization point and was essentially constant at 2 mol (i.e., dihydrate) at higher RH% levels.

CONCLUSIONS

This study has demonstrated for the first time that the inhalable trehalose microparticles and nanoparticles with different particle morphology were rationally designed and

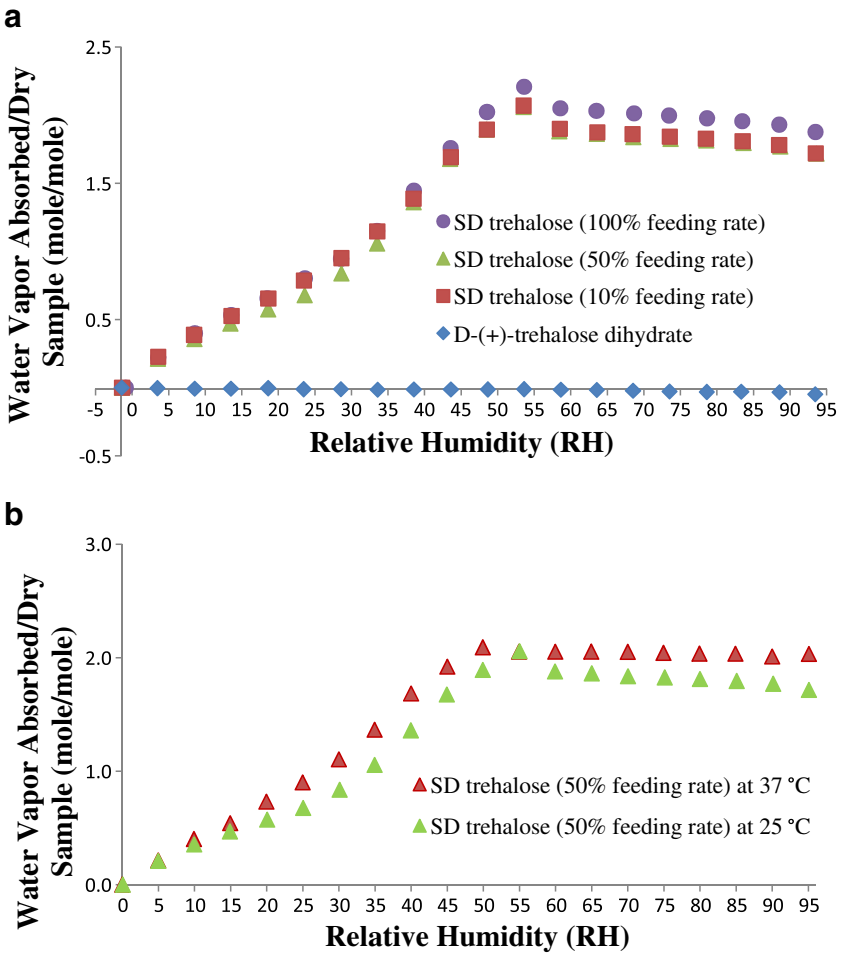

Fig. 9. Water vapor absorption isotherms of SD trehalose and raw trehalose dihydrate particles (water vapor absorbed/dry sample (mole/mole) *vs* relative humidity (*RH*)): **a** comparison of water vapor absorption between SD trehalose and raw trehalose dihydrate particles at 25°C; **b** comparison of water vapor absorption of SD trehalose particles (50% feeding rate) at 25°C and 37°C

successfully produced via organic solution advanced spray drying from dilute solution. The use of organic solvent has several important advantages to produce unimodal microparticulate/nanoparticulate inhalable powders with greatly reduced residual water content which can improve product stability and performance. The SD trehalose particles from various feeding rates possessed similar amorphous phase and capacity of water vapor sorption. Pharmaceutical processing conditions correlated in a meaningful manner with changes in important physicochemical and particle properties essential for targeted pulmonary delivery as DPIs. The thermotropic and lyotropic phase transition at 25°C and 37°C (biological temperature) were correlated with the amorphous glassy *vs*. rubbery state and solid-state phase transitions.

ACKNOWLEDGEMENTS

The authors gratefully acknowledge financial support from the UK Daniel P. Reedy Fellowship and Fellowship support from the UK Center of Membrane Sciences awarded to Xiaojian Li. The authors thank Dr. Dicky Sick Ki Yu for SEM access and Dr. Tonglei Li for XRPD and HSM access.

REFERENCES

1. Hickey AJ, Mansour HM. Chapter 5: delivery of drugs by the pulmonary route. In: Florence AT, Siepmann J, editors. Modern Pharmaceutics. 5th ed. New York: Taylor and Francis, Inc.; 2009. p. 191–219.
2. Katzenstein AL, Myers JL. Idiopathic pulmonary fibrosis: clinical relevance of pathologic classification. Am J Respir Crit Care Med. 1998;157(4 Pt 1):1301–15.
3. Sethi S, Sethi R, Eschberger K, Lobbins P, Cai X, Grant BJ, *et al*. Airway bacterial concentrations and exacerbations of chronic obstructive pulmonary disease. Am J Respir Crit Care Med. 2007;176(4):356–61.
4. Sexauer WP, Fiel SB. Aerosolized antibiotics in cystic fibrosis. Semin Respir Crit Care Med. 2003;24(6):717–26.
5. Park CW, Hayes DJ, Mansour HM. Pulmonary inhalation aerosols for targeted antibiotics drug delivery. Invited paper. European Pharmaceutical Review. 2011;16(1):32–6.
6. Rhee YS, Mansour HM. Nanopharmaceuticals I: nanocarrier systems in drug delivery. Invited paper. International Journal of Nanotechnology Special Issue-Nanopharmaceuticals. 2011;8(1/2):84–114.
7. Wu X, Mansour HM. Nanopharmaceuticals II: application of nanoparticles and nanocarrier systems in pharmaceutics and nanomedicine. Invited Paper. International Journal of Nanotechnology Special Issue-Nanopharmaceuticals. 2011;8(1/2):115–45.
8. Mansour HM, Rhee YS, Wu X. Nanomedicine in pulmonary delivery. International Journal of Nanomedicine. 2009;4 (December):299–319.
9. Patton JS, Byron PR. Inhaling medicines:delivering drugs to the body through the lungs. Nature Reviews Drug Discovery. 2007;6 (1):67–74.
10. Hickey AJ, Mansour HM. Chapter 43: formulation challenges of powders for the delivery of small molecular weight molecules as aerosols. In: Rathbone MJ, Hadgraft J, Roberts MS, Lane M, editors. Modified-release drug delivery technology. 2nd ed. New York: Informa Healthcare; 2008. p. 573–602.
11. Zeng XM, Martin GP, Marriott C. Particulate Interactions in Dry Powder Formulations for Inhalation. ed., New York, NY: Taylor & Francis, Inc.; 2001. p. 225.
12. Hickey AJ, Mansour HM, Telko MJ, Xu Z, Smyth HD, Mulder T, *et al*. Physical characterization of component particles included in dry powder inhalers. I. Strategy review and static characteristics. J Pharm Sci. 2007;96(5):1282–301.
13. Xu Z, Mansour HM, Hickey AJ. Particle interactions in dry powder inhaler unit processes. Journal of Adhesion Science and Technology Special Issue on Adhesion Aspects in Pharmaceutical Sciences. 2011;25(4/5):451–82.
14. Xu Z, Mansour HM, Mulder T, McLean R, Langridge J, Hickey AJ. Heterogeneous particle deaggregation and its implication for therapeutic aerosol performance. J Pharm Sci. 2010;99(8):3442–61.
15. Chacon M, Molpeceres J, Berges L, Guzman M, Aberturas MR. Stability and freeze-drying of cyclosporine loaded poly (D, L lactide-glycolide) carriers. Eur J Pharm Sci. 1999;8 (2):99–107.
16. Bosquillon C, Rouxhet PG, Ahimou F, Simon D, Culot C, Preat V, *et al*. Aerosolization properties, surface composition and physical state of spray-dried protein powders. J Control Release. 2004;99(3):357–67.
17. Abdelwahed W, Degobert G, Stainmesse S, Fessi H. Freeze-drying of nanoparticles: formulation, process and storage considerations. Adv Drug Deliv Rev. 2006;58(15):1688–713.
18. Lo YL, Tsai JC, Kuo JH. Liposomes and disaccharides as carriers in spray-dried powder formulations of superoxide dismutase. J Control Release. 2004;94(2–3):259–72.
19. Andya JD, Maa YF, Costantino HR, Nguyen PA, Dasovich N, Sweeney TD, *et al*. The effect of formulation excipients on protein stability and aerosol performance of spray-dried powders of a recombinant humanized anti-IgE monoclonal antibody. Pharm Res. 1999;16(3):350–8.
20. Garmise RJ, Staats HF, Hickey AJ. Novel dry powder preparations of whole inactivated influenza virus for nasal vaccination. AAPS PharmSciTech. 2007;8(4):article E81.
21. Crowe LM, Reid DS, Crowe JH. Is trehalose special for preserving dry biomaterials? Biophys J. 1996;71(4):2087–93.
22. Surana R, Pyne A, Suryanarayanan R. Effect of aging on the physical properties of amorphous trehalose. Pharm Research. 2004;21(5):867–74.
23. Fakes MG, Dali MV, Haby TA, Morris KR, Varia SA, Serajuddin AT. Moisture sorption behavior of selected bulking agents used in lyophilized products. PDA J Pharm Sci Technol. 2000;54(2):144–9.
24. Surana R, Pyne A, Suryanarayanan R. Effect of preparation method on physical properties of amorphous trehalose. Pharmaceutical Research. 2004;21:1167–76.
25. Moran A, Buckton G. Studies of the crystallization of amorphous trehalose using simultaneous gravimetric vapor sorption/near IR (GVS/NIR) and "modulated" GVS/NIR. AAPS PharmSciTech. 2009;10(1):297–302.
26. Moran A, Buckton G. Adjusting and understanding the properties and crystallisation behaviour of amorphous trehalose as a function of spray drying feed concentration. International Journal of Pharmaceutics. 2007;343(1–2):12–7.
27. Steckel H, Bolzen N. Alternative sugars as potential carriers for dry powder inhalations. International Journal of Pharmaceutics. 2004;270(1–2):297–306.
28. Bosquillon C, Lombry C, Preat V, Vanbever R. Influence of formulation excipients and physical characteristics of inhalation dry powders on their aerosolization performance. J Control Release. 2001;70(3):329–39.
29. Mansour HM, Xu Z, Hickey AJ. Dry powder aerosols generated by standardized entrainment tubes from alternative sugar blends: 3. Trehalose dihydrate and D-mannitol carriers. J Pharm Sci. 2010;99(8):3430–41.
30. Mansour HM, Hickey AJ. Raman characterization and chemical imaging of biocolloidal self-assemblies, drug delivery systems, and pulmonary inhalation aerosols. A review. AAPS PharmSciTech. 2007;8(4):Article 99 (E01-E16).
31. Vehring R. Pharmaceutical particle engineering via spray drying. Pharm Res. 2008;25(5):999–1022.
32. Masters K. Spray Drying Handbook. 5th ed. Longman Scientific & Technical, Wiley; 1991. p. 725.
33. Mansour HM, Zografi G. The relationship between water vapor absorption and desorption by phospholipids and bilayer phase transitions. Journal of Pharmaceutical Sciences. 2007;96 (2):377–96.

34. Horvat M, Mestrovic E, Danilovski A, Craig DQ. An investigation into the thermal behaviour of a model drug mixture with amorphous trehalose. Int J Pharm. 2005;294(1–2):1–10.
35. Jones MD, Hooton JC, Dawson ML, Ferrie AR, Price R. Dehydration of trehalose dihydrate at low relative humidity and ambient temperature. Int J Pharm. 2006;313(1–2):87–98.
36. Taylor LS, York P. Characterization of the phase transitions of trehalose dihydrate on heating and subsequent dehydration. J Pharm Sci. 1998;87(3):347–55.
37. Adi H, Traini D, Chan HK, Young PM. The influence of drug morphology on aerosolisation efficiency of dry powder inhaler formulations. J Pharm Sci. 2008;97(7):2780–8.
38. Adi S, Adi H, Tang P, Traini D, Chan HK, Young PM. Microparticle corrugation, adhesion and inhalation aerosol efficiency. Eur J Pharm Sci. 2008;35(1–2):12–8.
39. Marsac PJ, Rumondor AC, Nivens DE, Kestur US, Stanciu L, Taylor LS. Effect of temperature and moisture on the miscibility of amorphous dispersions of felodipine and poly(vinyl pyrrolidone). J Pharm Sci. 2010;99(1):169–85.
40. Takeuchi H, Yasuji T, Yamamoto H, Kawashima Y. Temperature- and moisture-induced crystallization of amorphous lactose in composite particles with sodium alginate prepared by spray-drying. Pharm Dev Technol. 2000;5(3):355–63.